ASTROBIOLOGY
Volume 20, Number 11, 2020

DOI: 10.1089/ast.2019.2038

Laboratory Analysis of Returned Samples from the AMADEE-18 Mars Analog Mission

Emmanuel Alexis Lalla,[1,2] Kristen Cote,[1,*] Dylan Hickson,[1] Stefanie Garnitschnig,[2] Menelaos Konstantinidis,[1] Pamela Such,[1] Christine Czakler,[2] Christian Schroder,[3] Alessandro Frigeri,[4] Maurizio Ercoli,[5] Anna Losiak,[2,6,7] Sophie Gruber,[2] and Gernot Groemer[2]

Abstract

Between February 1 and 28, 2018, the Austrian Space Forum, in cooperation with the Oman Astronomical Society and research teams from 25 nations, conducted the AMADEE-18 mission, a human–robotic Mars expedition simulation in the Dhofar region in the Sultanate of Oman. As a part of the AMADEE-18 simulated Mars human exploration mission, the Remote Science Support team performed analyses of the Dhofar area (Oman) in an effort to characterize the region as a potential Mars analog site. The main motivation of this research was to study and register selected samples collected by analog astronauts during the AMADEE-18 mission with laboratory analytical methods and techniques comparable with those that are likely to be used on Mars in the future. The 25 samples representing unconsolidated sediments obtained during the simulated mission were studied by using optical microscopy, Raman spectroscopy, X-ray diffraction, laser-induced breakdown spectroscopy, and laser-induced fluorescence spectroscopy. The principal results show the existence of minerals and alteration processes related to volcanism, hydrothermalism, and weathering. The analogy between the Dhofar region and the Eridana Basin region of Mars is clearly noticeable, particularly as an analog for secondary minerals formed in a hydrothermal seafloor volcanic-sedimentary environment. The synergy between the techniques used in the present work provides a solid basis for the geochemical analyses and organic detection in the context of future human–robotic Mars expeditions. AMADEE-18 has been a prime test bed for geoscientific workflows with astrobiological relevance and has provided valuable insights for future space missions. Key Words: Planetary exploration—Combined instrumentation methods—Astrobiology—Simulated space mission. Astrobiology 20, 1303–1320.

1. Introduction

AMADEE-18 was an integrated Mars analog mission conducted by the Austrian Space Forum in the Dhofar region in the Sultanate of Oman between February 1 and 28, 2018. The activities were carried out in the proposed terrestrial martian analog site and directed by a Mission Support Center in Innsbruck, Austria (Groemer *et al.*, 2019). During the planning stage of the mission, a sequential method for the detection of biomarkers for future human and robotic Mars missions was developed. Garnitschnig (2018) proposed a framework for the detection of potential biomarkers and compiled a list of potential test sites for future missions (Groemer, 2018; Groemer *et al.*, 2019). These kinds of methods and frameworks pursue a double objective with strong implications in the search of life on Mars and optimization in the synergy of analytical techniques at different test sites for future martian missions. The first objective was to evaluate the impact of carbon detection, water evidence, and characterize any biosignature. The second objective was the rational selection of techniques to be used, which was based on martian mission equipment suites as found on Mars 2020 and

[1]Centre for Research in Earth and Space Science (CRESS), York University, Toronto, Ontario, Canada.
[2]Austrian Space Forum, Innsbruck, Austria.
[3]Biological and Environmental Sciences, Faculty of Natural Sciences, University of Stirling, Scotland, United Kingdom.
[4]National Institute of Astrophysics, Institute for Space Astrophysics and Planetology IAPS, Rome, Italy.
[5]Dipartimento di Fisica e Geologia, Università degli Studi di Perugia, Perugia, Italy.
[6]Institute of Geological Sciences, Polish Academy of Sciences, Wrocław, Poland.
[7]WildFire LabHatherly Laboratories, University of Exeter, Exeter, United Kingdom
*Present address: Department of Physics, University of Toronto, Toronto, Canada.

ExoMars. Thus, the synergistic combination of analyses is of interest for target selection, deployment outcrop sites, and instrumentation capabilities for water and possible life detection (Garnitschnig, 2018; Gruber *et al.*, 2019; Stromberg *et al.*, 2019).

Several *in situ* experiments were used during this study such as the FieldSpec and ScanMars systems, which utilize reflectance spectroscopy and ground-penetrating radar (described in detail in this issue). Other laboratory-based techniques that we have used during our analysis are microimaging, Raman spectroscopy, X-ray diffraction (XRD), laser-induced breakdown spectroscopy (LIBS), and laser-induced fluorescence (LIF). The objective of these methods is to have a full biological and geological understanding of the surface. In this work, we present the results of the analysis done using laboratory-based techniques and illustrate how they can be used to qualitatively and quantitatively describe landscapes *in situ*, in addition to analyzing samples collected by humans during analog and/or actual space missions. This may facilitate the inference of a surface's suitability for subsequent analyses. For example, the laboratory techniques can help in future selection of instrumentation and design of the workflow for a possible field survey.

The main motivation of this research was to study selected samples collected by analog astronauts during the AMADEE-18 mission with laboratory analytical methods and techniques proposed in the strategic framework developed by Garnitschnig (2018) for the AMADE-18 mission and comparable with the techniques that will be used on Mars in the future. The analyses were performed at the Planetary Exploration Instrumentation Laboratory at York University and the Royal Ontario Museum, both in Toronto, Canada. The results and measurements exemplify the capabilities of each technique, and the combined advantages. Furthermore, the results emphasize the selection applicability of portable twin systems—those that resemble real flight instruments used in past/present/future martian missions and based on the same technology—for future analog missions. Table 1 compares laboratory-based rover instrumentation from past, current, and future missions. Finally, scanning electron microscopy (SEM), energy dispersive spectroscopy (EDS), and XRD as described above can be used to validate field experiments such as LIBS, Raman spectroscopy, and LIF.

1.1. Methods used in this study and their relevance to Mars studies

Raman spectroscopy is a nondestructive spectroscopic technique that does not require sample preparation. The technique is well suited for *in situ* analyses of rocks and minerals, and has been used for mineral identification and organic detection of the target sample (Ferraris *et al.*, 2012; Edwards *et al.*, 2013). Raman spectroscopy has been proposed as a method for geological identification of Mars-related materials, and will be used during the future martian missions SuperCam and Scanning Habitable Environments with Raman and Luminescence for Organics and Chemicals (SHERLOC) (NASA Mars 2020) or the European Space Agency's (ESA)-Raman Laser Spectrometer System (ExoMars) (Beegle *et al.*, 2015; Wiens *et al.*, 2016; Rull *et al.*, 2017).

LIBS utilizes emissions from plasma created at the surface of a sample through high-power laser pulses to perform quantitative chemical analyses (Wiens *et al.*, 2012). One of the primary benefits of LIBS is that there is no required sample preparation before measurement and only optical access to the sample is required. This makes it a formidable candidate for standoff chemometric analysis (Cremers and Radziemski, 2013; Konstantinidis *et al.*, 2019). For these reasons, LIBS was selected for flight on Curiosity in the Chemistry and Camera (ChemCam) instrument (Anderson *et al.*, 2015), and will fly on Mars 2020 (Wiens *et al.*, 2016).

LIF provides a method for organic and mineral detection through excitation of molecules by the absorption of laser light followed by spontaneous emission of light (Storrie-Lombardi *et al.*, 2009). Typically, LIF used to be understood as an undesired byproduct of a Raman measurement,

Table 1. Comparison of the Capabilities of the Five Systems Employed in This Investigation

Laboratory technique	*Mineral identification*	*Elemental composition*	*Organic detection*	*Geological context*	*Laboratory instrumentation location in this study*	*Rover instrument equivalent*
Raman spectroscopy	Yes	Potentially (only major elements)	Yes	Yes (mapping)	Royal Ontario Museum	RLS (ExoMars) SuperCam (Mars 2020) SHERLOC (Mars 2020)
Microimaging	Yes	No	Yes	Yes	York University	CLUPI (ExoMars)
XRD	Yes	No	No	Potentially	Royal Ontario Museum	CheMin (MSL)
LIBS	No	Yes	Potentially	Yes (mapping)	York University	ChemCam (MSL) SuperCam (Mars 2020)
LIF	Potentially	No	Yes	No	York University	SHERLOC (Mars 2020)
SEM–EDS	Yes (imaging)	Yes (qualitative)	Yes	No	York University	

XRD = X-ray diffraction; LIBS = laser-induced breakdown spectroscopy; LIF = laser-induced fluorescence; SEM = scanning electron microscopy; EDS = energy dispersive spectroscopy; RLS = Raman Laser Spectrometer; ChemCam = Chemistry and Camera; SHERLOC = Scanning Habitable Environments with Raman and Luminescence for Organics and Chemicals; CheMin = Chemistry and Mineralogy; MSL = Mars Science Laboratory.

but Eshelman *et al.* (2018) have shown it to be useful for detection of organics such as organic carbon and amino acids. SuperCam and SHERLOC (NASA Mars 2020 Rover) will also incorporate this technique in their search for evidence of past or present life on Mars (Beegle *et al.*, 2015; Wiens *et al.*, 2016). SHERLOC utilizes LIF as a supporting tool for selection of targets with possible organics through fast mapping. Subsequently, Raman spectroscopy will be able to determine the mineralogy and possible existence of biosignatures (Beegle *et al.*, 2015).

XRD allows the user to obtain mineral identification and structural characterization and it is commonly used for crystallography and mineralogy (Klein, 2008). In space, ChemMin, onboard the Mars Science Laboratory (MSL) Curiosity rover, combines XRD with X-ray fluorescence (Bish *et al.*, 2013). The ChemMin system can identify and quantify the minerals present in rocks and soil to understand the habitability of Mars.

Other supportive methods such as SEM–EDS allow us to analyze the mineralogical composition, which, in combination with the *in situ* petrological description and in laboratory optical mineralogy study, provides information about regolith material source, petrological composition, identification of weathering and hydrothermal processes affecting the martian rocks. A summary of the techniques used to determine mineral and elemental composition, detect organics, and deduce the geological context is presented in Table 1.

2. Geology of the Site and Its Analogy with Mars

In the Dhofar region, a prerift, synrift, and postrift sequence that ranges from Upper Cretaceous prerift sediments to Upper Middle Miocene postrift deposit units can be found. These series involve three sedimentary groups (Roger *et al.*, 1989): the Hadhramaut Group, Paleocene to late Eocene in age that overlays in unconformity over Cretaceous strata consisting of shallow-marine carbonate units (Lepvrier *et al.*, 2002); The Dhofar Group, late Eocene, laying unconformably over Hadhramaut Group represented by two limestones units part of shallow lacustrine to shallow-marine deposits (Lepvrier *et al.*, 2002); and the Fars Group, early Miocene, composed of conglomerated and carbonate deposit units (Lepvrier *et al.*, 2002). Figures 1 and 2 show the Paleocene–Miocene stratigraphic units of the Dhofar region simplified geological map of southern Oman (Dhofar area) [from Robinet *et al.* (2013)].

In the study area, the geological records registered by outcrops of the Huqf Supergroup in the North-East elongated salt basin in south Oman were uplifted blocks become sites of carbonate deposition, whereas basinal transtensional depressions were overlain with black shale and silicyte (Amthor *et al.*, 2005). These belong to the Ara Fm depositional times (Ramseyer *et al.*, 2013) as can be observed in Fig. 3.

Quaternary deposits of alluvial fans were found during the field study. These unconsolidated sediments are present together with outcrops ranging from approximately several cm to

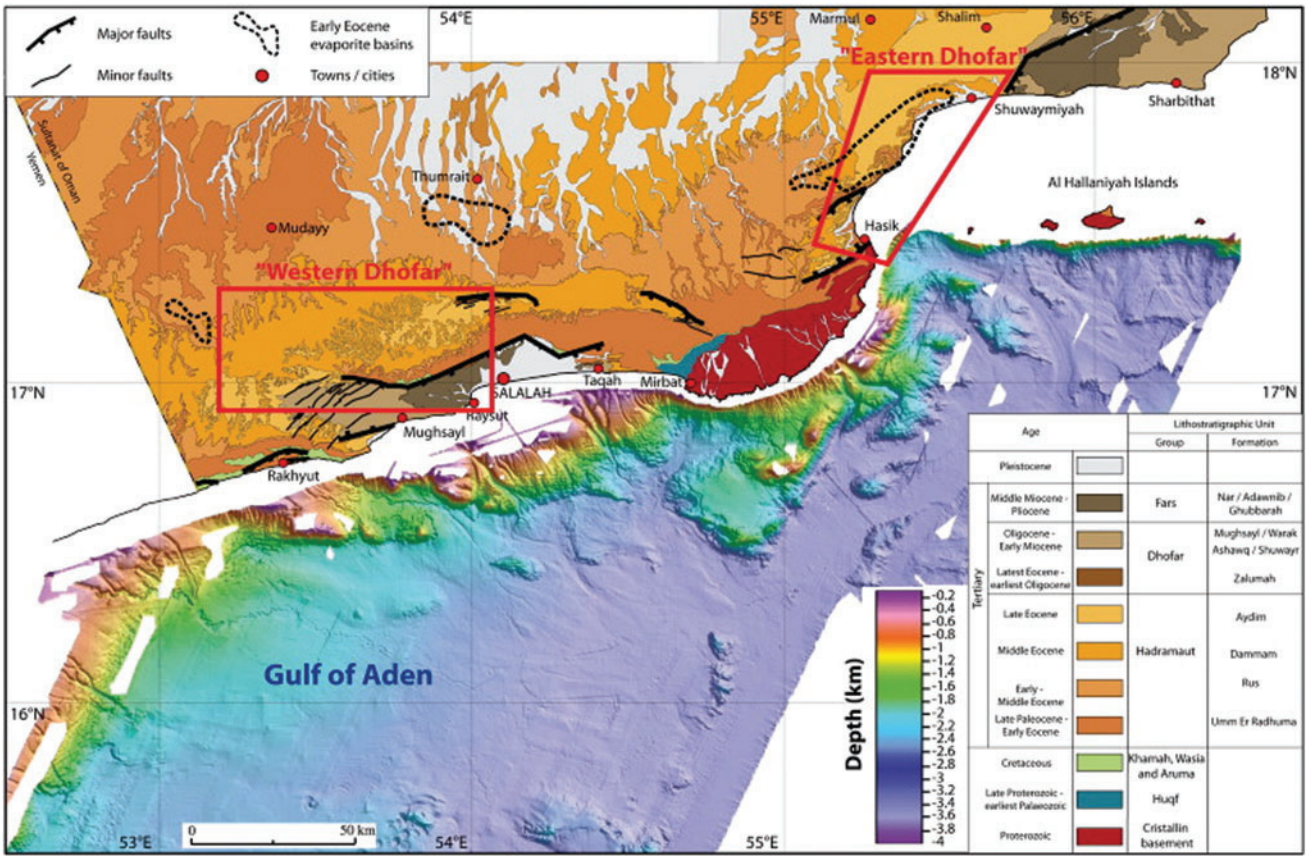

FIG. 1. Simplified geological map of southern Oman (Dhofar area) showing the two studied areas discussed in this article from Robinet *et al.* (2013) (reproduced with permission of Elsevier). Color images are available online.

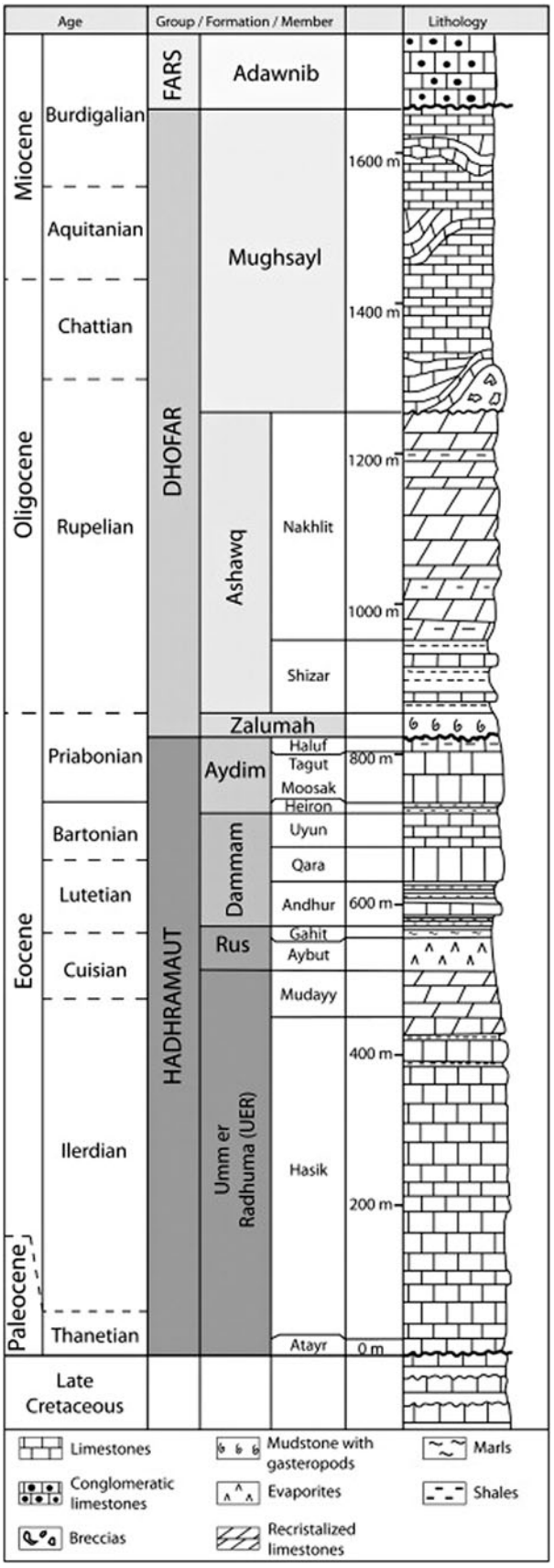

FIG. 2. The Paleocene–Miocene stratigraphic units of the Dhofar region from Robinet *et al.* (2013) (reproduced with permission of Elsevier).

1 m of silicified dolomites and organic-rich laminated chert (silicilyte) belonging to the Ara Fm as observed in Fig. 3. The alluvial fans are composed mostly of sand, pebbles, and boulders cemented by poorly sorted rolled clasts covered by thin dark oxidized coating (Yuan *et al.*, 2016) (Fig. 3).

The feeding area of the sediments for the alluvial fans comes from the northwest-north region created by the erosion and weathering of the Oman mountain outcrops and the Huqf Supergroup sediments.

Part of the unconsolidated sediments of the alluvial deposits includes volcanic rocks of alkaline to basaltic composition belonging to the volcanic rocks interbedded with the Precambrian–Cambrian deposits, limestones, silicified dolomite fragments, and fragments of hydrothermally altered silicified dolomite carbonates and volcanic rocks that include magnetite and sulfides like the remnant product of the hydrothermalism observed before in the Oman mountains (Reuning *et al.*, 2007).

The hydrothermalism was vaguely studied in the Dhofar area. It is believed to be related to magmatism in part with the intrusion of late-stage veinlets carrying metals of magnetite and sulfides. A possible supergene alteration was also identified in the samples during the petrological description and field studies with secondary mineralization of alunite, coesite, and montmorillonite in the sediments together with oxides and secondary chlorite.

The synrift deposits observed in the regolith and in the Ara Fm could correspond to possible martian analogues. The Precambrian–Cambrian carbonates interbedded with volcanic products and the development of hydrothermal deposits due to active magmatism in a spreading region from the study area can be correlated to similar regions from the surface of Mars as reported by Michalski *et al.* (2017). For example, Eridania Basin shows a 3.8 billion-year record from a spreading area with active high magmatism and signatures of high Mg–Fe rich clay mineral products of hydrothermalism in an ancient lake base with high content of carbon and Ca–Fe–Mg rich carbonates (Michalski *et al.*, 2017). Even though the chemistry of Eridania Basin on Mars is still unknown, strong evidence from infrared spectroscopy and high-resolution imaging suggests that the Eridania Basin contains a complex suite of alteration minerals that likely formed in a hydrothermal seafloor volcanic-sedimentary setting with intrusions of sulfide-rich fluids interacting with ultramafic–mafic volcanic rocks and sediments (Michalski *et al.*, 2017). Even so, more areas in the martian surface show similarities to geological records from selected places of ancient Earth (Léveillé, 2009). Therefore, our future understanding of martian geochemistry and ancient development of organic-rich carbon deposits in similar environments can be improved with the study of these analogues on Earth.

3. Experimental Analysis and Setup

In total, 25 geological samples, mostly consisting of various unconsolidated sediments, were collected by the analog astronauts at the different locations where the *in situ* experiments were carried out throughout the AMADEE-18 mission (Fig. 4a, b). The locations in which samples were collected and the field cataloging procedures were conducted are presented in the Field Activity Plans from the

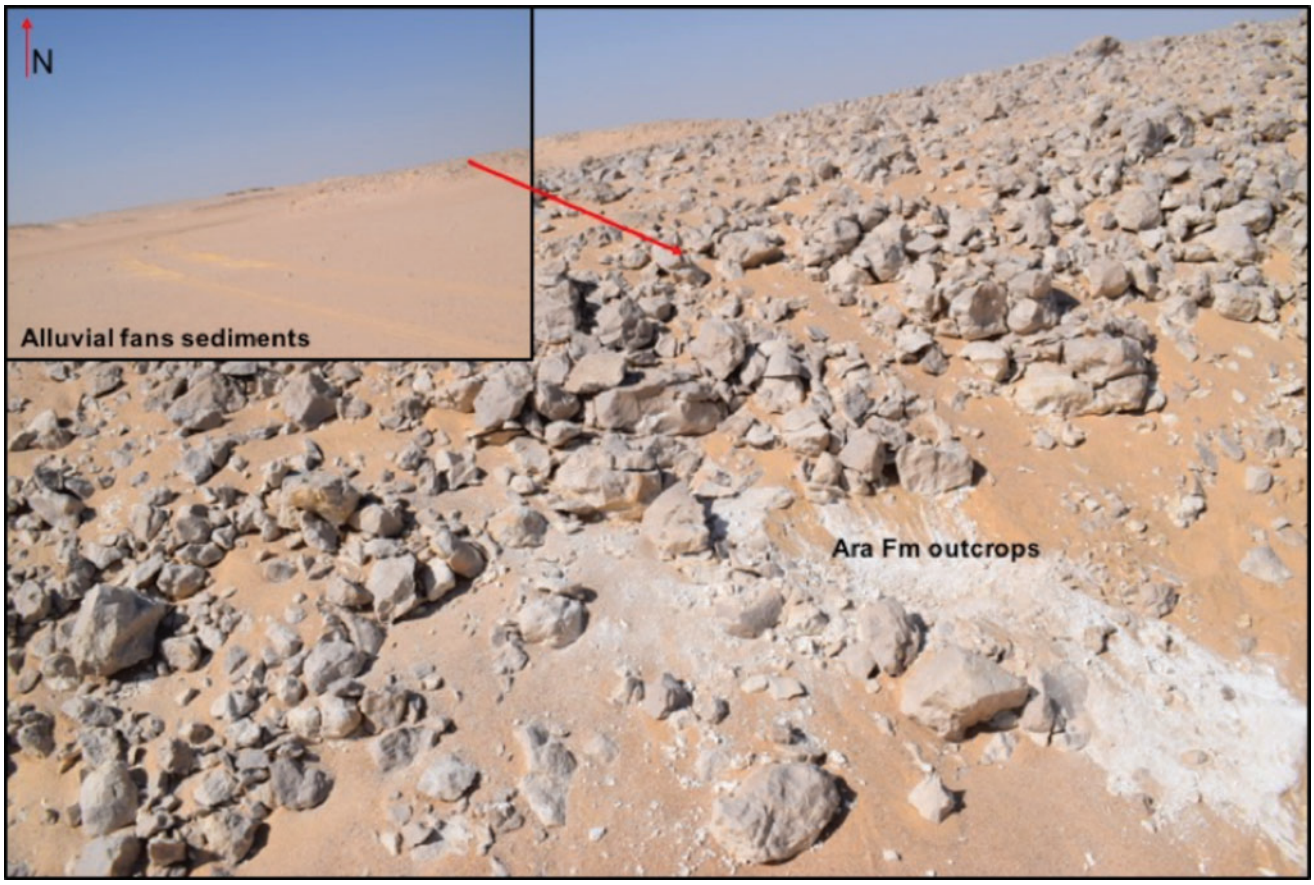

FIG. 3. Picture of the field site showing the outcrops and alluvial fans deposits where samples were taken and studied in the laboratory. Color images are available online.

mission (Groemer, 2018; Sejkora *et al.*, 2018). The detailed geographical positions of the geosampling are available in the Online Supporting Data.

The samples were composed of unconsolidated sediments with grain sizes ranging from 25 μm to a few millimeters in diameter. For practical reasons, LIBS and SEM–EDS measurements need to have a pelletized sample before carrying out the measurements. The sample preparation was conducted to ensure the same mineral and organic compositional properties. A small amount (5–10 g) from each sample was powdered manually in an agate mortar and sieved to obtain particles ranging from 45 to 150 μm in size. Powders were mixed with 1 mL of distilled water and compressed. These humidified pellet samples were left to dry by evaporation at high vacuum and room temperature. This resulted in the formation of stable pellets. To carry out the measurements, the pellet was glued to a microscope slide for easy handling (Fig. 4c).

Micro-Raman measurements were made with a Horiba Lab-RAM Aramis Raman spectrometer. The analyses employed a 532 nm 50 mW laser focused to a 1.3 μm spot full width half max (FWHF). The spectrometer configuration used a 100 μm slit and a 1200 grooves/mm diffraction grating. The location of the points to be analyzed was selected by the operator, along with several automatic mappings. A total of 40 different points per sample were acquired. The routine for obtaining the spectra was as follows: selecting the point, taking a preview spectrum (fast measurement for good signal and focusing condition), and finally acquiring the spectra. The measurement conditions (acquisition and accumulations) for the manual location were varied from point to point ranging from several seconds to several minutes. The automatic mapping conditions per sample were 20 points separated by 0.05 cm. Measurements at each point involve a cumulative spectrum of five 10 s exposures. Spectra were corrected following the standard procedure available on the OPUS software from Bruker. A background subtraction was done by using the Rubberband correction method and 65 baseline points. The normalization to the maximum value = 1 was carried out, and spectral smoothing was used when the spectra were noisy for band identification. The Levenberg–Marquardt curve fitting was done in some of the spectra because several Mineral Raman bands were overlapping. Mineral identification was performed by comparison with the RRUFF Database using Crystal Sleuth (Laetsch and Downs, 2006; Downs *et al.*, 2015). Voight fittings were used to deconvolve the main spectral features when the Raman bands of several minerals overlapped.

XRD measurements were carried out with a Bruker D8 Advance Diffractometer equipped with a two-circle goniometer setup and CuK_{α} radiation source. The system was operated with a voltage generator of 40 kV and current of 40 mA. The data were collected with a Ni-filter, low

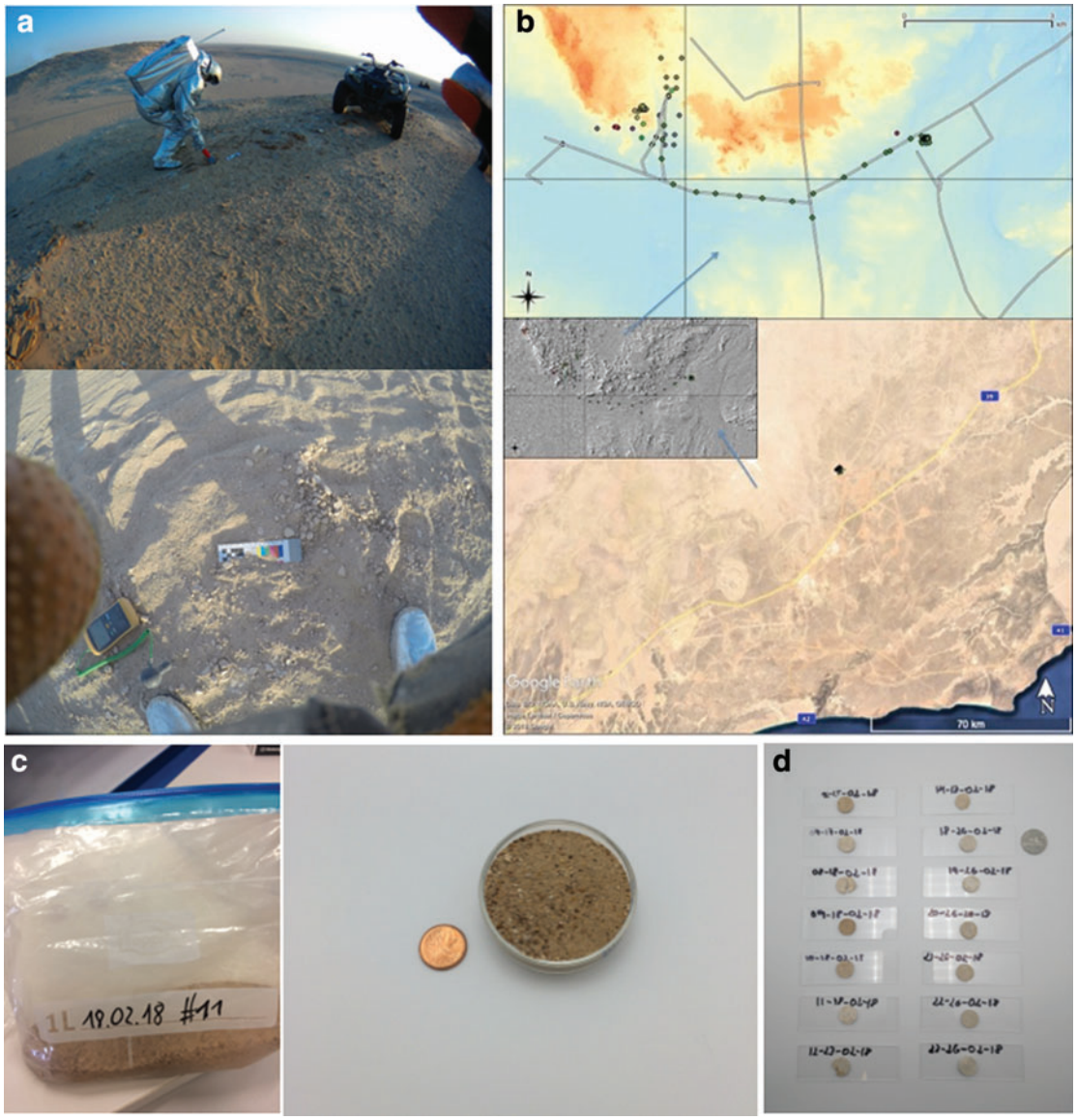

FIG. 4. **(a)** Analog astronauts doing a geosampling in the field during the AMADEE-18 mission; **(b)** DEM map of the sampling points with the location, and DEM (the coordinates of sampling location are on the Supporting Data); **(c)** example of one of the geosamples cataloged at York University; and **(d)** pelletized sand samples. DEM, digital model elevation. Color images are available online.

background plate, and a LYNXEYE detector. The XRD diffractograms were acquired in the range $10 < 2\theta° < 70$ with a step size of 0.02° and acquisition time of 1 s per step and a rotation spin of 15 per minute. Analysis of resulting diffractograms was performed with the XPowder 2004.04.71 software with PDF-2 (2010) and the American Mineralogist Crystal Structure Database crystallographic databases. A background correction for each diffractogram was achieved with the Splin-autoroller and polynomial tools available XPowder 2004.04.71 that allows for calculation of a background polynomial subtraction function (Martin, 2004). XRD mineral quantification and theoretical density determination of the mixture were achieved by using the reference intensity ratio from pattern matching results with XPowder 2004.04.71 (Martin, 2004).

The microimaging analyses and petrological descriptions were made with a standard binocular Zeiss microscope.

Laser-induced fluorescence measurements were carried out with a 266 nm Raman-LIF system designed by Eshelman *et al*. (2014, 2015), satisfying selected requirements of a putative flight-worthy instrument. The excitation power was provided by a quadrupled Team Photonics diode-pumped solid state Nd:YAG laser with a 0.6 ns pulse width and 13.8 μJ pulse energy at 1000 Hz. The acquisition system was composed of an Andor Shamrock 163 spectrometer. A 600 lines/mm grating allowed for an observation window between 270 and 550 nm. The spectrometer is coupled to an intensified, cooled charge-coupled device (CCD) (Andor iStar 334T). The 1 cm long, 20-point LIF measurements include each an accumulation of 40 spectra with 0.01 s exposures. The spectral corrections were done in the same way as the Raman analysis.

The elemental composition of the AMADEE-18 geosamples was measured with a Vega TESCAN SEM equipped with a Bruker Quantax energy dispersive X-ray (EDS) detector. The beam voltage used for secondary electron imaging and backscattered electron imaging (BSE), as well as EDS spectra acquisition, was 10 kV. SEM–EDS data were collected on the pelletized sand samples without any coating.

LIBS measurements were achieved with a breadboard system. Plasma excitation was obtained with a 1064 nm Quantel ULTRA Nd:YAG laser with 10 mJ pulse energy and 10 ns pulse width, focused to a 33 μm spot (FWHM). The peak power density at the target is on the order of 100 GW/cm^2. The light produced from the plasma is collected through an off-axis f/7 collection system and delivered through fiber to the Andor ME5000 echelle spectrograph combined with the ICCD Andor iStar 334T camera (covering 230–850 nm). The spectrometer was wavelength calibrated with an Ocean Optics HG1 Calibration Light Source and intensity calibrated with an Ocean Optics DH-3P-CAL Calibration Light Source. Pelletized samples were used for LIBS analysis. Each LIBS measurement consists of 15 cumulative spectra with 0.1 s exposures (one spectrum per laser shot, for a total of 15 shots). An intensity correction was performed by using the standard ANDOR Solis software procedure for the ME5000. Identification of element present within the spectra was carried out with the Solis software and manual identification with the NIST Spectral Lines Database (National Institute of Standards and Technology, 2016).

4. Results

4.1. Field samples petrological description

Fourteen of the most representative regolith samples were selected to describe the mineralogy and petrology. These samples included: 1) Quaternary alluvial fans sediments, 2) silicified veinlets intruding Ara Fm outcrops, and 3) the silicified dolomite and carbonate rock samples from the Ara Fm outcrops. These studies were later used to compare with the data acquired from LIBS, Raman, and SEM–EDS laboratory analyses.

A microscope magnifier Zeiss lens was used for the petrological description. Varying grain sizes from sand to pebbles and gravel were observed (Figs. 5 and 6).

During the petrological study of the sediment samples, sand and pebble sizes of calcite, dolomite, silicified dolomite rocks, and quartz rock fragments were observed. These present rounded to subrounded shapes with sizes up to 1 mm. All of them show an irregular oxidized coating on their surfaces. They represent more of the 80% of the sediment components.

In minor quantities, <10%, subrounded to subangular fragments of volcanic rocks from intermediate to basic composition (andesites and basalts) are present. These rocks mostly show an altered matrix, with presence of secondary clay alteration (possible montmorillonite and coesite), plagioclase, amphiboles, pyroxenes crystal observed embedded in matrix.

Sediments also show single crystals in <8% and 0.5–0.1 mm sizes range belonging to unidentified feldspars in angular to subangular crystals; unidentified plagioclases, prismatic subangular crystals, many of them with clay alteration on their borders. Volcanic quartz subrounded to rounded with dark inclusions, prismatic crystals of amphiboles, chloritized and with presence of oxides inclusions on their borders, and transverse basal sections of pyroxenes, prismatic crystal of chlorite and zircons were also identified.

Between 2% and 5% oxides and sulfides were present in the sediments. Alunite was observed as a likely replacement of sulfides and pyrite, in small sizes (<0.5 mm) of silicified veinlets (Figs. 5 and 6).

Samples belonging to silicified veinlets and silicified dolomite Ara Fm sediments were also described. The first ones show a matrix of fine microcrystalline white silica, with presence of anorthoclase plagioclase crystals in sizes ranging from <0.1 mm up to 0.5 mm, which were fractured and rotated, showing evidence of flow movement in the matrix. Magnetite and sulfides were also observed. For the silicified dolomite rock fragments, a fine microcrystalline matrix of dolomite replaced by silica was clear through microscope mineral identification. Some of them show a small zebra pattern, related to possible hydrothermal activity as can be observed in Figs. 5 and 6.

4.2. Raman analysis

The mineralogical composition results are listed in Table 2 following the ordering of Dana's classification method (Palache *et al.*, 1952). Figure 7 shows representative Raman spectra obtained from the samples. Identification of mineral species is achieved by using the RRUFF Database within the Crystal Sleuth software (Laetsch and Downs, 2006; Downs *et al.*, 2015). The following references for each mineral were considered alongside the spectral analyses: oxides (Balachandran and Eror, 1982; Wang *et al.*, 2004; Markovski *et al.*, 2017), carbonates (Rull-Perez and Martinez-Frias, 2003; Buzgar and Apopei, 2009), pyroxenes (Huang *et al.*, 2000; Wang *et al.*, 2001), feldspar (Freeman *et al.*, 2008; Lalla *et al.*, 2015, 2019), clays (Apopei and Buzgar, 2010; Lalla *et al.*, 2016; Black and Hynek, 2018), and organics (Ferrari, 2007). The organics present in the main Raman bands in the range of 2800 to 3000 cm^{-1} correspond to C–H bonding, and the other less intense bands $\sim$1300 cm^{-1} correspond to C–C vibrations (Beegle *et al.*, 2015).

4.3. XRD analysis

The minerals found within the collected samples when using XRD are compiled in Table 3. Figure 8 compiles the XRD diffractograms of the different sampling points, and the higher concentration minerals detected on the different samples are also indexed in the figure. The detailed mineral quantification of each transect point is attached as Supporting Data in weight percent (wt %) including all the minor minerals.

4.4. Laser-induced fluorescence

A 1 cm long, 20-point LIF measurement was carried out on unprocessed sediment. Results of the LIF measurements for the different sampling points are shown in Fig. 9a–d. The most intense LIF bands for organic detection are located between 300 and 450 nm (Eshelman *et al.*, 2014, 2015). The spectra from the organics detected at the collected samples were compared with the internal Planetary Exploration

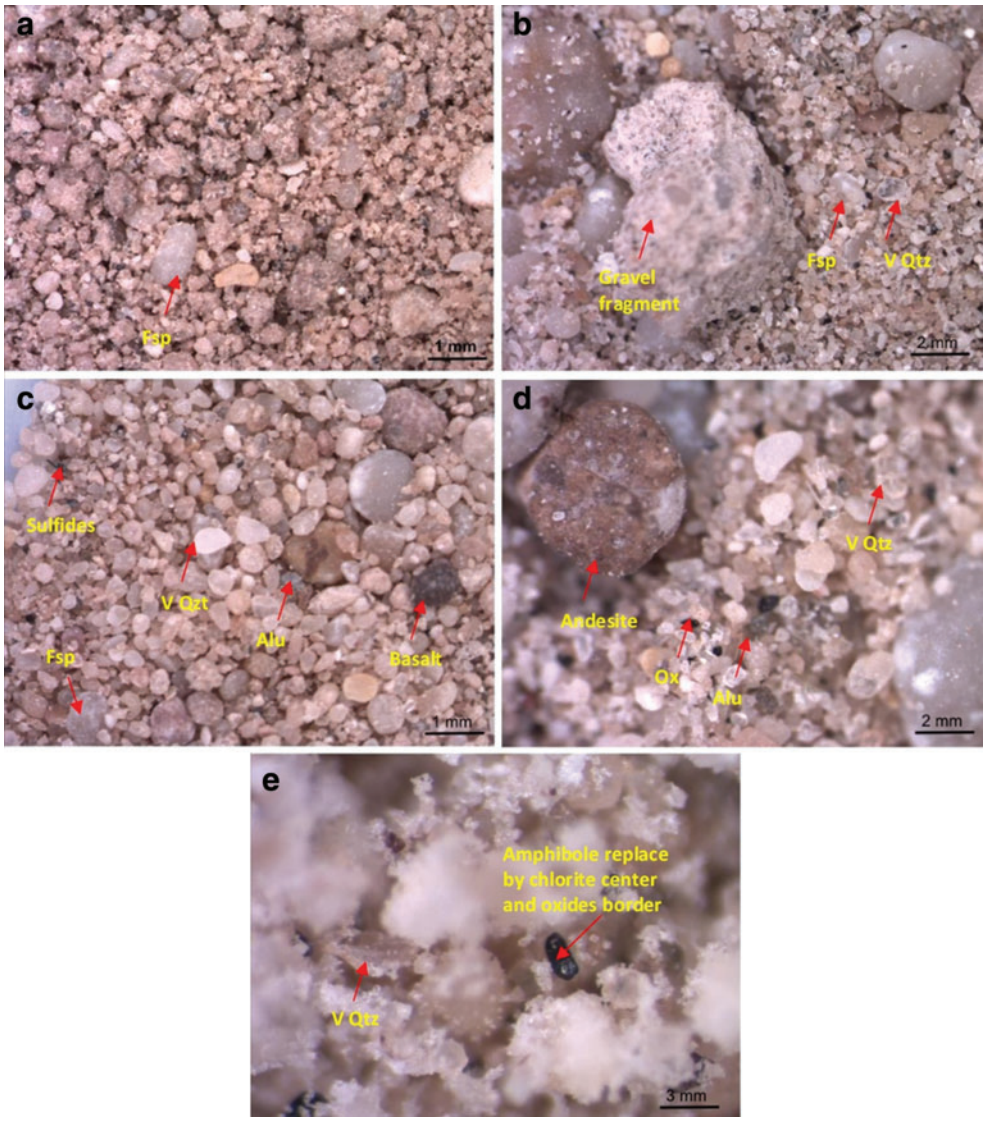

FIG. 5. Magnified images of the alluvial fan sediments and sand to gravel size material. **(a)** Dolomites, silicate, carbonate clasts with feldspar (Fsp) crystals; **(b)** sand with presence of volcanic quartz (V Qtz), feldspar, disseminated oxides (Ox) and gravel size clast; **(c)** rounded volcanic quartz, dolomite clasts, rounded basalt clast and alunite (Alu) and feldspar crystals; **(d)** andesite subrounded clast with abundant presence of volcanic quartz, and oxides (Ox) and disseminated alunite crystals; **(e)** amphibole in fine-grained silica with chloritized mineralization in center and oxides in borders. Color images are available online.

Instrumentation Laboratory (PIL) database (Cote *et al.*, 2018; Lymer, 2018). The results coincide with previous analyses of amino-acids-like tyrosine and possibly tryptophan. Figure 9e shows a comparison between the different amino acids used as standards and the detected organics from AMADEE-18 mission. The minerals detected coincide with carbonates (dolomite and calcite) and silica (quartz) LIF spectra from the PIL database. The dolomite is clearly differentiable on the spectra considering broad bands at ~350 and ~460 nm. The quartz presents a weak band at ~325 and the strongest broad band between 450 and 475 nm. Also, Fig. 9e presents some selected bands from the different minerals detected and AMADEE-18 results. Table 4 shows the minerals and organic signature detected for the different samples. The minimum amount of minerals and organic signatures was considered only for >15% of detection of the 20-point, being in >3 points

4.5. SEM analysis (SEM–EDS)

The results of the semiquantitative EDS analyses are summarized in Table 5. The elemental analysis, representing bulk composition of the mixed powder samples, was performed on areas of ~10 mm^2 on each pellet representing a qualitative approximation of the elemental distribution. The quantification of EDS spectra was performed with the P/B-ZAF QUANTAX analysis strategy (Bruker-Nano, 2011). This is a standard less, self-calibrating spectrum analysis procedure that makes use of ZAF matrix correction formulas, enabling simple processing of the EDS spectra collected

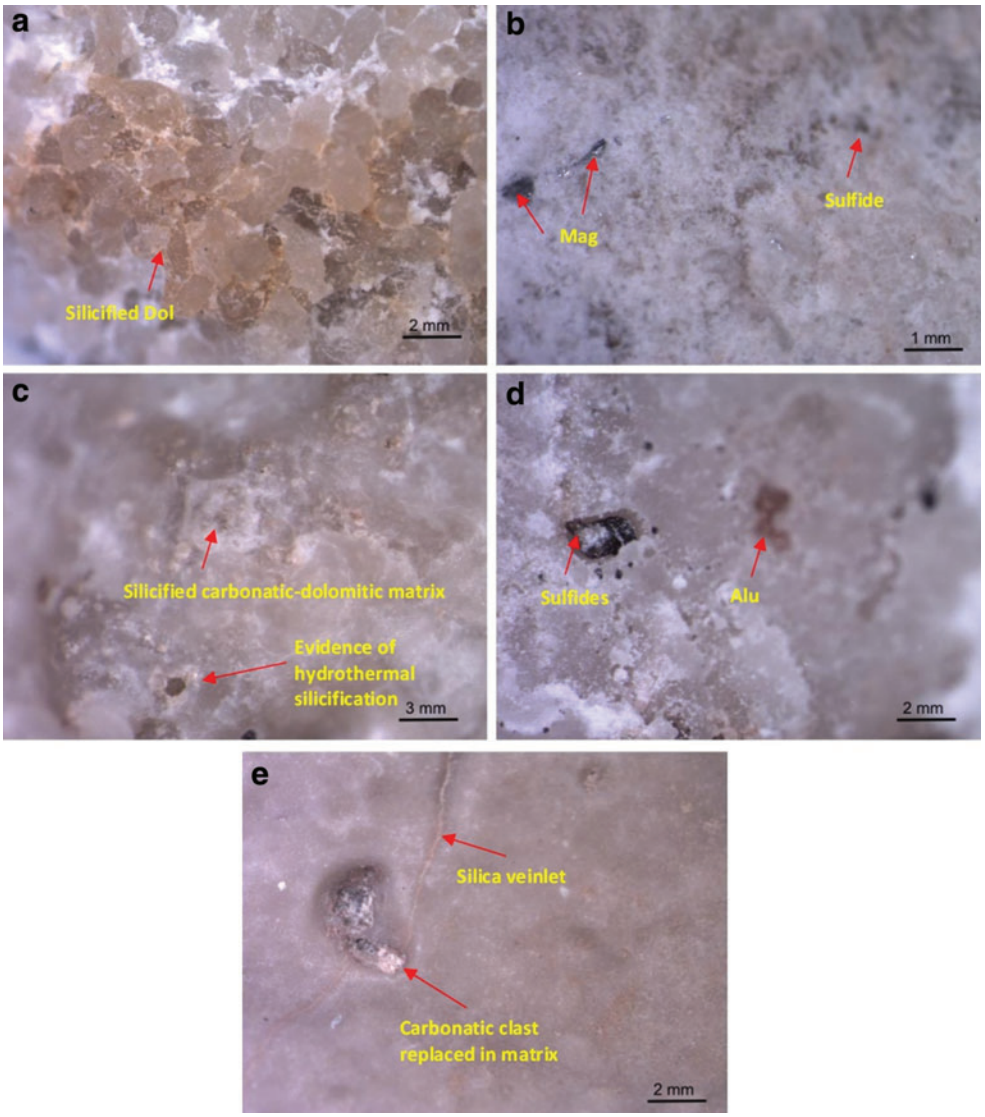

FIG. 6. Magnified images of the alteration processes. **(a)** The silicate replacing dolomite (Dol) rock from Ara Fm with oxide coating on the surface; **(b)** silica vein intruded in Ara Fm carrying magnetite (Mag) and sulfides; **(c)** silicate replacing carbonate rocks from Ara Fm (possible evidence of supergen activity); **(d)** random dissemination of oxides and alunite (Alu) crystals in silica vein matrix; **(d)** fine to very fine silica matrix replacing carbonate rocks (details of carbonate clast and silica veins in process of replacement can be observed). Color images are available online.

for each sample. Since the accuracy of EDS quantification is relatively low, especially with standardless quantification, the normalized elemental mass percentages were used to allow comparison within and between samples for the relative elemental concentrations. With these quantifications, a qualitative analysis of the sample elemental composition was performed on the data. Figure 10 shows an example of the elemental distribution and BSE profile of a sample. Most samples appeared relatively homogeneous in BSE images; however, distinct mineral phase boundaries appeared in some samples, as evidenced in the BSE image and corresponding EDS spectral map of samples 5–17. The stark contrast seen between the left and right halves of both images is a result of large sodium chloride grains, interpreted as halite. The EDS spectra of the soil samples were more homogeneous across all samples, reflecting the random mixing involved in their preparation. The wt % oxide concentrations (rounded to the nearest percentage to reflect the low accuracy of method) in Table 5 were calculated from the normalized mass percentages derived through the quantification procedure. All of the elemental iron present was converted to wt % FeO (Supporting Data).

The spectra for some samples gave erroneous results, likely due to the large error associated with the quantification, and only the elements with identifiable peaks were quantified. Two poor quality spectra (4–15 and 8–18) have been omitted in Table 5.

4.6. Laser-induced breakdown spectroscopy

LIBS spectra are shown in Fig. 11. The spectral range covers almost all the near ultraviolet (UV), visible, and near infrared. The main compositional elements—Al, Ca, Ti, Si, K, Fe, and Mg—were identified by using the NIST Spectral

TABLE 2. MICRO-RAMAN MINERAL AND OTHER MATERIAL DETECTION ON THE DIFFERENT SAMPLING POINTS FROM AMADEE-18 MISSION

Mineral	*Samples*														
	4–15	*5–17*	*7–17*	*8–18*	*9–18*	*10–18*	*11–18*	*12–23*	*14–13*	*18–26*	*19–26*	*20–26*	*21–26*	*22–26*	*23–26*
Magnetite	X	X				X		X		X			X	X	X
Hematite						X		X	X	X	X			X	X
Goethite						X									
Anatase		X					X				X	X		X	
Chromite												X			
Quartz	X	X	X	X	X	X	X	X	X	X	X	X	X	X	X
Calcite	X	X	X	X	X	X	X	X	X	X	X	X	X	X	X
Dolomite		X						X					X		
Titanite						X									
Olenite												X			
Enstatite		X									X				
Diopside							X				X				
Epidote													X		X
Microcline				X				X						X	
Orthoclase													X		
Sanidine				X	X	X	X					X			
Albite		X			X	X		X	X		X	X	X		X
Andesine					X			X			X				
Labradorite	X														X
Clays						X									
Carbonaceous material and organics	X	X	X	X	X	X	X	X	X	X	X	X	X	X	X

X indicates that the mineral was found to be present in the respective sample.

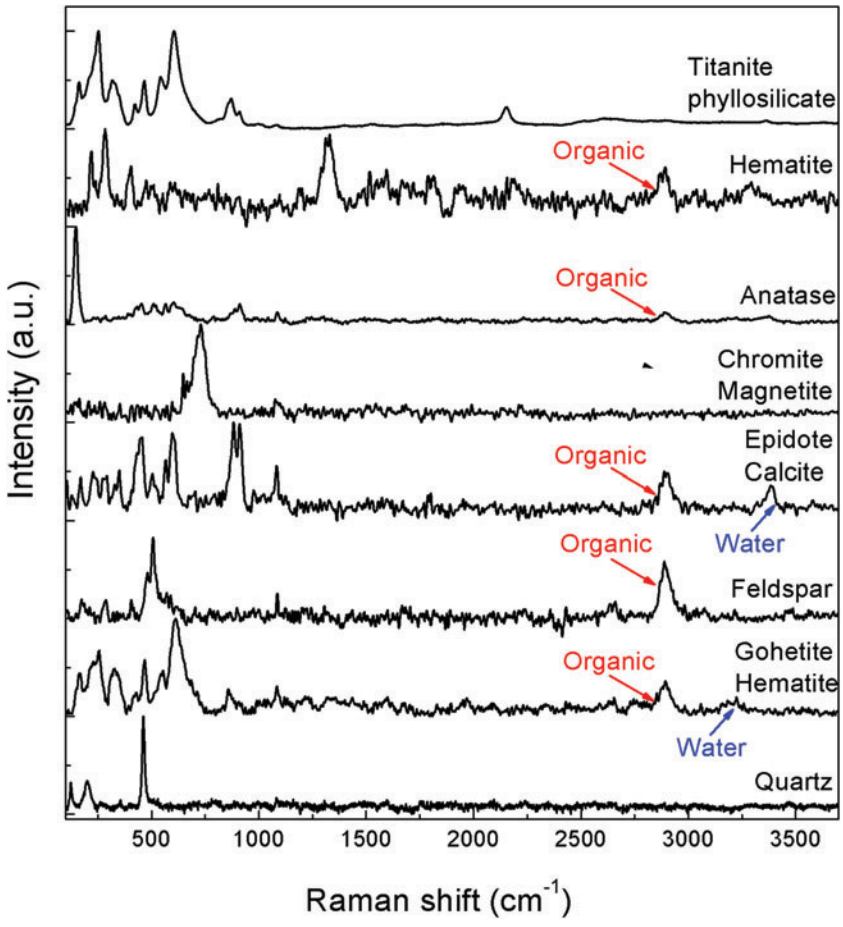

FIG. 7. Micro-Raman spectra of the most significant mineral phases detected. Color images are available online.

Table 3. X-Ray Diffraction Mineral Detection on the Different Sampling Points from AMADEE-18 Mission

Mineral	*Samples*													
	4–15	*7–17*	*8–18*	*9–18*	*10–18*	*11–18*	*12–23*	*14–13*	*18–26*	*19–26*	*20–26*	*21–26*	*22–26*	*23–26*
Iron oxides					X									
Anatase	X												X	
Rutile	X												X	
Quartz		X	X	X	X	X	X		X	X	X	X	X	X
Calcite		X	X	X	X	X	X	X	X	X	X	X	X	X
Dolomite		X	X	X		X				X				
Ferrosilite								X				X		
Olenite											X			
Diopside	X													
Pigeonite							X							
Enstatite			X					X						
Epidote														X
Pyrope			X								X			
Coesite							X							
Olivine						X			X					
Feldspar									X					X
Anorthoclase													X	
Orthoclase				X										
Sanidine							X							
Anorthite					X					X				
Albite	X		X	X				X				X		
Bytownite											X			
Andesine	X	X												
Labradorite	X							X						

X corresponds to the detected mineral in each collected sample.

Lines Database (National Institute of Standards and Technology, 2016). In the near-UV region, the most intense peaks are Ca II located at 315.89, 317.93, 393.36, and 396.85 nm, Al I peaks at 308.31 nm, and Ti II within the 310–360 nm region, and 368.5 nm. Si II peaks are present at 385.6 and 390 nm approximately, as well as Fe I peaks at 370.73 and 373.8 nm. The region from 480 to 660 nm contains Mg I (517.2 and 518.3 nm), Fe I and Fe II (526.6, 527, and 534.97 nm), Ca I (487.81 and 585.74 nm), and Na I (588.9 and 589.59 nm) characteristic lines. In the region of the nearinfrared, the major peaks observed correspond to Ca I (714.8, 720.2, and 732.6 nm), K I (doublet at 766.49 and 769.89 nm), and O I (777.4 and 844.6 nm).

5. Discussion

The petrological study of these samples shows evidence of hydrothermal deposits in the Ara Fm previously undescribed. This hydrothermalism is probably related to the syn–rift volcanism in the late stage of formation (Reuning *et al.*, 2007; Ramseyer *et al.*, 2013; Rollinson *et al.*, 2014). It is represented by the existence of the silica veinlets carrying sulfides and oxides intruding the dolomitic rocks studied in the present work. Part of this alteration has generated secondary clays being observed in the present samples. Also, a supergene alteration has been observed on the samples reflected by an oxidized coating over the surface of almost all the clasts described. These alterations are supported by the presence of tertiary clays. In general, the supergene alteration was produced by the alluvial water intruding into the outcrops from the surface. The supergene process is combined with other alterations like the weathering and the alteration of the postrift processes. All of the alteration processes described above are believed to have occurred on Mars. Because of this, this area has been proposed as a key terrestrial Mars analog for alteration processes (Chevrier and Mathé, 2007). The hydrothermalism and supergene alteration observed in the samples are comparable with similar geological data identified by the NASA MSL-Curiosity mission in Mars (Marzo *et al.*, 2010; Le Deit *et al.*, 2013; Popa *et al.*, 2015).

The spectroscopic analyses performed here detected minerals ranging from oxides to complex clays. The detected minerals match those observed when using optical microscopy. The detected carbonates such as dolomite and calcite correspond to the hydrothermal alteration. The oxides such as hematite and quartz are also significant in the context of understanding the hydrothermal processes. Also, minerals from old volcanism of the region such as pyroxene, feldspar, and olivine were detected. The meteoric alterations have also been detected in the form of clays and the water content on certain samples. The present results also confirm that Raman spectroscopy is able to detect certain mineral species that are not visually differentiable such as olenite, pyrope, or coesite minerals. Also, the results agree with the mineralogy previously reported (Amthor *et al.*, 2005; Ramseyer *et al.*, 2013). The other powerful application of the Raman analysis was the detection of organic materials on the different samples. However, the measurements must be complemented with the capabilities of other laser techniques to get semiquantitative concentrations of the organics present. Given the fast measurements and high sensitivity to target

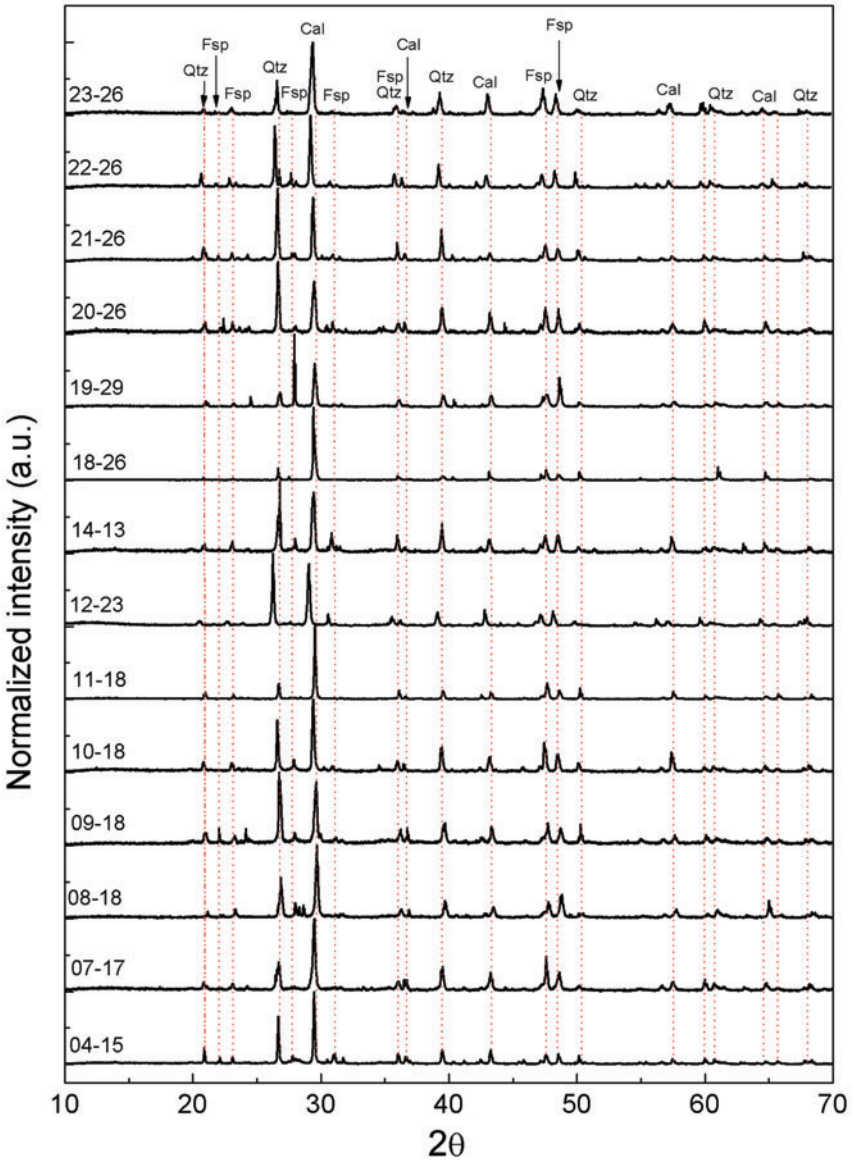

FIG. 8. X-Ray diffractogram of the selected transect points from the AMADEE-18 Mission. The minerals shown are the higher concentrations obtained from the quantification (see Supporting Data). Qtz, quartz; Cal, calcite; Fsp, feldspar. Color images are available online.

biomolecular structures that are present in the different samples, the best complementary method for detection of organics is LIF. The wavelength range for the detected organics matches the range for amino acids such as lysine or phenylalanine (Eshelman *et al*., 2014, 2018). Also, the LIF method helped to confirm the existence of carbonates such as calcite or dolomite and quartz.

The XRD measurements identified and quantified the mineralization present in the different samples. Indeed, the pattern matching facilitated easy identification of quartz, feldspars, and carbonates. The detection of some feldspars such as albite helped to confirm the hydrothermal alterations. Other minerals (pyroxene and certain feldspars) confirmed the existence of past volcanic activities. The high concentration of carbonates in the analyzed samples was confirmed with LIF, LIBS, and EDS. The high concentration of calcite and dolomite agrees with the petrological description of the sedimentary rocks.

The LIBS technique mainly detected Ca, Mg, Al, and other metal ions such as Fe. These elements could be the cations in the identified carbonates (*e.g.*, dolomite and calcite). However, Mg and Fe could also be associated with the volcanic parent mineralogy such as pyroxene, olivine, or Fe-oxides (magnetite). This agrees with the Si detected on the samples, which could represent the ionization of the pyroxene, olivine, and feldspars. Peaks corresponding to Al can be assigned to the different alkali–feldspar and/or clay mineralization present along all the different sampling points. The K and Na peaks probably belong to feldspar group minerals because this mineral group presents higher concentrations of K and Na compared with other minerals.

The semiquantitative EDS analysis of the uncoated pellets detected high concentrations of Si, Ca, and C, which is consistent with the dominant mineralogy of calcite, dolomite, and quartz determined through the other experimental techniques applied to the samples. Throughout the laboratory analysis, samples were handled with gloves and stored in sealed containers to minimize contamination. Despite these efforts, it is likely that some of the C measured by EDS for the samples is due to contamination; however, high

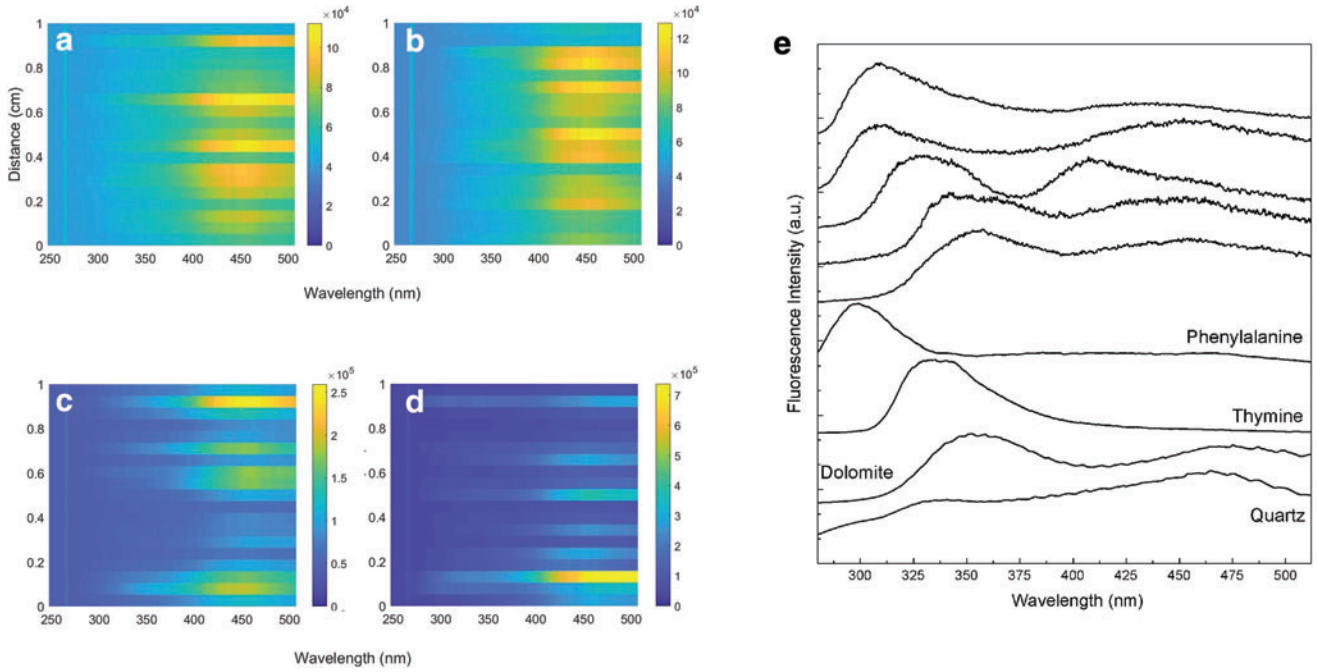

FIG. 9. Representative laser-induced fluorescence measurements (20 points along a 1 cm line) from the different sampling points from AMADEE-18: **(a)** 9–18; **(b)** 10–18; **(c)** 12–23; **(d)** 18–26; **(e)** selected spectral comparison with some organics and minerals. Color images are available online.

concentrations of ~40% indicate that contamination cannot be the only responsible mechanism, and that the presence of carbonates is probable. Possible contamination factors could include *in situ* biological contamination, or sample handling at the Kepler base station during the mission. Abed *et al.* (2010) reported that the bacterial community in the region is mainly composed of cyanobacterium (*e.g.*, Deltaproteobacteria, Bacteriodetes, Gemmatimonadetes, and Planctomycetes). However, we have shown that EDS provided a relatively quick and semi-nondestructive mineralogical and geochemical analysis of samples, with elemental results consistent with those derived from the other instruments.

From an astrobiological perspective, carbonates are most commonly associated with potentially habitable zones such as hydrothermal areas, marine or lacustrine sediments, or biominerals (Bish *et al.*, 2013). The carbonates form not only through hydrothermal or diagenetic processes, but they can have an origin of weathering byproducts or from serpentinization as well. Carbonates provide an energy source for chemosynthetic microbes on Earth. Considering the magnesium–iron rich carbonates detected by the Spirit rover (Morris *et al.*, 2010), the sand studied during the AMADEE-18 mission is a good geological candidate for an *in situ* instrument analysis of future space-qualified equipment prototypes and twin systems for future research.

The approach described in this section provides a geochemical instrumentation and methodological suite for the comprehensive analysis of a sample, yielding a mineralogical, elemental, organic, petrological, and geomorphological investigation. The results obtained from the different techniques illustrate the applicability of portable systems based on the real flight instruments for future analog missions (Lalla *et al.*, 2016; Sehlke *et al.*, 2019; Warren-Rhodes *et al.*, 2019). Further, the combined measurements of this

Table 4. Main Laser-Induced Fluorescence Mineralogical Detection for the Different Sampling Points from AMADEE-18 Mission (20-Point Mapping of 1 cm Line)

	Samples													
	4–15	*7–17*	*8–18*	*9–18*	*10–18*	*11–18*	*12–23*	*14–13*	*18–26*	*19–26*	*20–26*	*21–26*	*22–26*	*23–26*
Silicate (quartz, amorphous sand)	X	X	X	X	X	X	X	X	X	X	X	X	X	X
Carbonates (calcite or dolomite)	X	X	X					X	X	X	X	X	X	
Organic signature[a]	X	X		X	X	X	X	X			X	5	X	X

X corresponds to the detected mineral in each collected sample.
[a]The carbonate and organic signatures were considered only for >15% of detection—>3 points.

Table 5. Energy Dispersive Spectroscopy Elemental Quantification Converted to Equivalent Weight Percent Oxides for the Different Sampling Points from the AMADEE-18 Mission

	Samples												
Oxide wt %	*7–17*	*9–18*	*10–18*	*11–18*	*12–23*	*14–13*	*18–26*	*19–26*	*20–26*	*21–26*	*22–26*	*23–26*	*Average (oxide wt %)*
SiO_2	24	41	33	16	28	32	27	12	22	31	28	28	27
Al_2O_3	5	9	7	2	5	6	5	3	4	6	5	5	5
FeO	2	4	3	1	2	3	1	1	2	3	2	2	2
MgO	3	8	5	2	3	5	3	2	3	5	4	3	4
CaO	27	13	21	34	27	22	20	28	28	23	18	29	24
Na_2O	1	1	1	0	1	1	1	0	1	0	1	1	1
K_2O	1	1	1	1	1	1	1	1	1	2	1	1	1
CO_2	37	23	29	44	33	30	42	53	39	30	41	31	39
Total	100	100	100	100	100	100	100	100	100	100	100	100	103

Powder sample spectra collected over $\sim 10\,mm^2$ acquisition areas and normalized.

comprehensive geochemical suite in analog space missions will yield insight into how our present methods can be improved upon for future missions to Mars and beyond. Particularly, given the large degree of instrument overlap and complementation, continuous use of the geochemical suite in space exploration will facilitate a unique combination in which the instruments ought to be used (Foing *et al.*, 2011; Sehlke *et al.*, 2019; Warren-Rhodes *et al.*, 2019).

Among the possible proposed objectives, the suite of used laboratory techniques demonstrated that these analyses provided us useful information when the ''Selection of Instrumentation'' comes. Moreover, how the capabilities of these specific instruments in the terrestrial analog are not necessarily reflective of the true capabilities of the instruments in the martian context. Rather, we strive to demonstrate how the synthesis of information derived from the aforementioned instruments (whose techniques are highly comparable with those in present and future missions) can be used to maximize mineralogical, petrological, and astrobiological inference in a rigorous and efficient way. When the traverse plan is included in the workflow, this feature information could help determine (1) the logical orders of experiments according to the relevance of the acquired data; (2) duration of the experimental procedure (*e.g.*, how much time and how many astronauts are required, time lining, among others); and (3) risk assessments from landing site geomorphology, required sensing range, and energy duties (robotic and human).

As we have discussed over the course of the article, there are great mineralogical and astrobiological implications from studying terrestrial analogs, not only from the point of view of instrumentation validation but also in systematizing

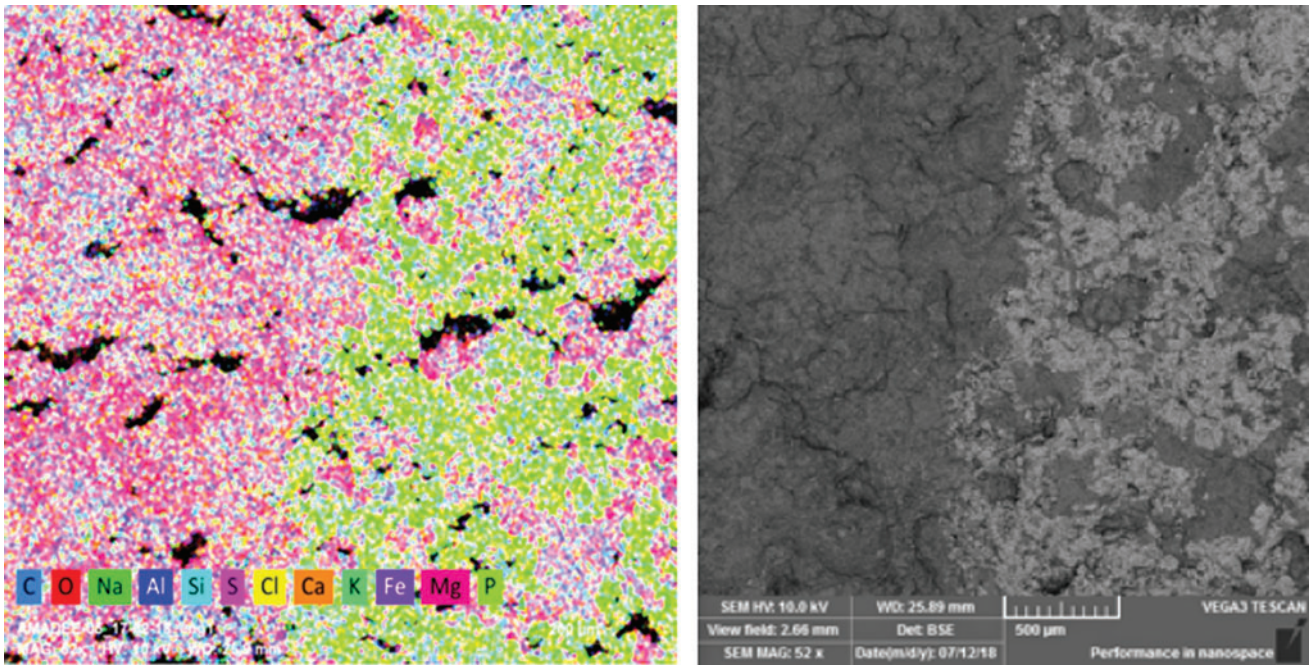

FIG. 10. An EDS elemental map of 5–17 (right). The left half of the image is primarily composed of oxygen, silicon, and calcium, whereas the right is dominated by sodium and chlorine. BSE image corresponding to area of EDS elemental map (left). BSE, backscattered electron imaging; EDS, energy dispersive spectroscopy. Color images are available online.

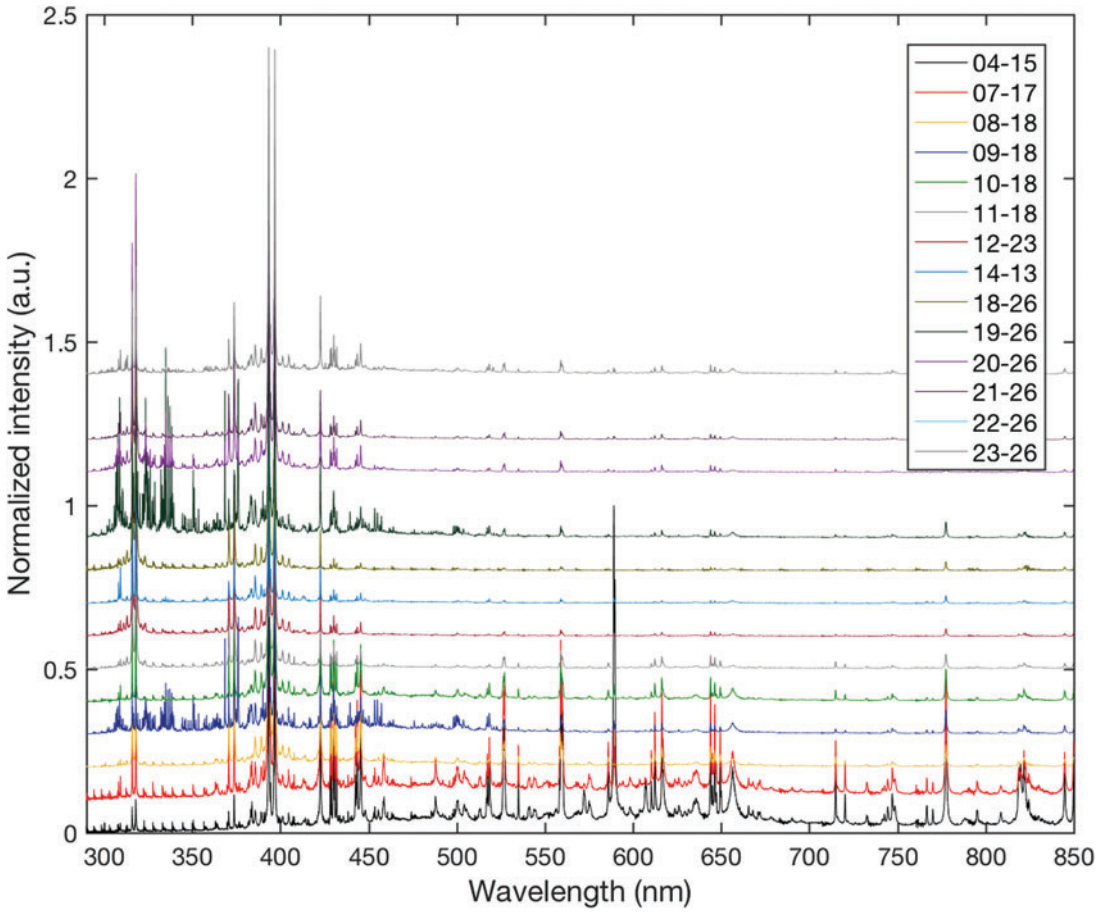

FIG. 11. Laser-induced breakdown spectroscopy spectra from the pelletized AMADEE-18 sand samples. Color images are available online.

methods of inference in the analog context, in addition to the setting of real space exploration. Indeed data come at many stages in space exploration, ranging from site selection, standardization of surrounding factors (such as passive reflectance), to the final mineralogical and astrobiological conclusions. Having accepted this, the only feasible way in which the utility of subsequent missions can be optimized is by having the integral processes and methods for inference rigorously established in the terrestrial domain. This is particularly true as we begin to travel with higher frequency beyond Mars.

6. Conclusion

1. The different techniques proposed in this work facilitated the petrological, mineralogical, and chemistry goals, chemical determination, and organic detection for possible habitability within the framework in martian research. These analyses are presented to provide guidance for future analog missions such as the AMADEE-18 mission. Also, the combined analytical methods will improve the methods and protocols in the detection of life for future space systems and Human missions to Mars.
2. The petrological analysis allowed us to determine the mineralogy, and geochemical origin of the minerals and alteration processes such as volcanism, hydrothermalism, and weathering, and to propose this area as a Mars analog for future field simulated missions and instrumental experimentation for samples study.
3. The mineral identification obtained from Raman spectroscopy and XRD agrees with the petrological analysis. The results show that the mineralogy of the different samples is dominated by the carbonates, silica (quartz), and feldspars.
4. The LIBS detection of Al, Ca, Ti, Si, K, Fe, Si, and Mg and the subsequent elemental analysis obtained by SEM–EDS were in high agreement. The detected elements could be assigned to carbonates, clays, Fe-ores, and feldspar. These results give the understanding of the elemental distribution between mineral phases detected by Raman and XRD.
5. The LIF measurements detected a high concentration of carbonates as did the EDS, XRD, LIBS, and Raman.
6. The detection of the organic samples was mainly achieved by Raman spectroscopy and LIF. Thus, the combined Raman-LIF measurements would provide the capabilities to identify organics on Mars.

Acknowledgments

The authors thank The Austrian Space Forum (OWF) and the AMADEE-18 Oman National Steering Committee, in particular Dr. Saleh Al-Shidhani and the government and people of the Sultanate of Oman. They are grateful to

Dr. K. Tait and V. Di Cecco for providing the opportunity to carry out measurements at the Royal Ontario Museum (ROM) and for their excellent support. Also, they thank Prof. M.G. Daly for his support and the opportunity to carry out measurements at the Planetary Exploration Instrumentation Laboratory (PIL), York University. E.A.L. expresses gratitude to The Ontario Centre of Excellence (OCE) for the TalentEdge Postdoctoral Funding. Figures 1 and 2 (Robinet *et al.*, 2013) have been reproduced with permission of Elsevier and proceeded by Copyright Clearance Center (Order contract 4673711500026). Finally, they also thank the anonymous reviewers and editor for their helpful and constructive comments and support during the review process that contributed to improving the final version of the article.

Author Disclosure Statement

No competing financial interests exist.

Supporting Data

The complete details of the measurements and results presented in the current research article can be found online in the OeWF Multi-Mission Science Data Archive of AMADEE-18 Mission at https://mission.oewf.org/archive/

Funding Information

There are no sources of funding for this work.

References

Abed, R.M.M., Al Kharusi, S., Schramm, A., and Robinson, M.D. (2010) Bacterial diversity, pigments and nitrogen fixation of biological desert crusts from the Sultanate of Oman. *FEMS Microbiol Ecol* 72:418–428.

Amthor, J.E., Ramseyer, K., Faulkner, T., and Lucas, P. (2005) Stratigraphy and sedimentology of a chert reservoir at the Precambrian-Cambrian boundary: the Al Shomou Silicilyte, South Oman Salt Basin. *GeoArabia* 10:89–122.

Anderson, R., Bridges, J.C., Williams, A., Edgar, L., Ollila, A., Williams, J., Nachon, M., Mangold, N., Fisk, M., Schieber, J., Gupta, S., Dromart, G., Wiens, R., Le Mouélic, S., Forni, O., Lanza, N., Mezzacappa, A., Sautter, V., Blaney, D., Clark, B., Clegg, S., Gasnault, O., Lasue, J., Léveillé, R., Lewin, E., Lewis, K.W., Maurice, S., Newsom, H., Schwenzer, S.P., and Vaniman, D. (2015) ChemCam results from the Shaler outcrop in Gale crater. *Mars Icarus* 249:2–21.

Apopei, A.I. and Buzgar, N. (2010) The Raman study of amphiboles. *Analele Stiint ale Univ ''Al I Cuza'' din Iasi Geol* 56:57–83.

Balachandran, U. and Eror, N.G. (1982) Raman spectra of titanium dioxide. *J Solid State Chem* 42:276–282.

Beegle, L., Bhartia, R., White, M., Deflores, L., Abbey, W., Wu, Y.H., Cameron, B., Moore, J., Fries, M., Burton, A., Edgett, K.S., Ravine, M.A., Hug, W., Reid, R., Nelson, T., Clegg, S., Wiens, R., Asher S., and Sobron, P. (2015) SHERLOC: scanning habitable environments with Raman and luminescence for organics and chemicals. *IEEE Aerospace Conference Proceedings*, Big Sky, MT, USA, [Epub ahead of print]; DOI: 10.1109/AERO.2015.7119105

Bish, D.L., Blake, D.F., Vaniman, D.T., Chipera, S.J., Morris, R. V, Ming, D.W., Treiman, A.H., Sarrazin, P., Morrison, S.M., Downs, R.T., Achilles, C.N., Yen, A.S., Bristow, T.F., Crisp, J.A., Morookian, J.M., Farmer, J.D., Rampe, E.B., Stolper, E.M., Spanovich, N., and Team, M.S.L.S. (2013) X-ray diffraction results from Mars Science Laboratory: mineralogy of Rocknest at Gale Crater. *Science* 341: 1238932.

Black, S.R. and Hynek, B.M. (2018) Characterization of terrestrial hydrothermal alteration products with Mars analog instrumentation: implications for current and future rover investigations. *Icarus* 307:235–259.

Bruker-Nano (2011) *Introduction to EDS Analysis: Reference Manual, DOC-M82-EX*. Bruker Nano GmbH, Berlin, Germany.

Buzgar, N. and Apopei, A.I. (2009) The Raman study on certain carbonates. *Analele Stiint ale Univ ''Al I Cuza'' Iasi* 55: 97–112.

Chevrier, V. and Mathé, P.E. (2007) Mineralogy and evolution of the surface of Mars: a review. *Planet Space Sci* 55:289–314.

Cote, K., Lalla, E., Daly, M., and Tait, K. (2018) Characterization of a combined raman, lif, and libs system with time resolved fluorescence capabilities for planetary exploration applications. *Women in Planetary Science and Exploration (WPSE) Conference*, Toronto, Canada.

Cremers, D.A. and Radziemski, L.J. (2013) *Handbook of Laser-Induced Breakdown Spectroscopy*. John Wiley and Sons Ltd., Oxford, United Kingdom.

Edwards, H.G.M., Hutchinson, I.B., Ingley, R., Parnell, J., Vítek, P., and Jehlička, J. (2013) Raman spectroscopic analysis of geological and biogeological specimens of relevance to the ExoMars mission. *Astrobiology* 13:543–549.

Eshelman, E., Daly, M.G., Slater, G., Dietrich, P., and Gravel, J.F. (2014) An ultraviolet Raman wavelength for the in-situ analysis of organic compounds relevant to astrobiology. *Planet Space Sci* 93–94:65–70.

Eshelman, E., Daly, M.G., Slater, G., and Cloutis, E. (2015) Time-resolved detection of aromatic compounds on planetary surfaces by ultraviolet laser induced fluorescence and Raman spectroscopy. *Planet Space Sci* 119:200–207.

Eshelman, E., Daly, M.G., Slater, G., and Cloutis, E. (2018) Detecting aromatic compounds on planetary surfaces using ultraviolet time-resolved fluorescence spectroscopy. *Planet Space Sci* 151:1–10.

Ferrari, A.C. (2007) Raman spectroscopy of graphene and graphite: disorder, electron-phonon coupling, doping and nonadiabatic effects. *Solid State Commun* 143:47–57.

Ferraris, G., Dubessy, J., Caumon, M.-C., and Rull, F., editors. (2012) *Raman Spectroscopy Applied to Earth Sciences and Cultural Heritage*. Mineralogical Society of Great Britain and Ireland, England.

Foing, B.H., Stoker, C., Zavaleta, J., Ehrenfreund, P., Thiel, C., Sarrazin, P., Blake, D., Page, J., Pletser, V., Hendrikse, J., Direito, S., Kotler, J.M., Martins, Z., Orzechowska, G., Gross, C., Wendt, L., Clarke, J., Borst, A.M., Peters, S.T.M., Wilhelm, M.-B., Davies, G.R., and Team, I.E. (2011) Field astrobiology research in Moon–Mars analogue environments: instruments and methods. *Int J Astrobiol* 10:141–160.

Freeman, J.J., Wang, A., Kuebler, K.E., Jolliff, B.L., and Haskin, L.A. (2008) Characterization of natural feldspars by raman spectroscopy for future planetary exploration. *Can Mineral* 46:1477–1500.

Garnitschnig, S. (2018) *Development of a Supportive Method for the Detection of Biomarkers During Future-Robotic Mars Missions*. University of Inssbruck and Space Austrian Forum.

Groemer, G. (2018) *AMADEE-18 Mission Report*. Austrian Space Forum, Inssbruck, Australia.

Groemer, G., Gruber, S., Uebermasser, S., Soucek, A., Lalla, E., Lousada, J., Sams, S., Sejkora, N., Garnitschnig, S., and Sattler, B. (2019) The AMADEE-18 Mars Analog Expedition in the Dhofar region of Oman. *Astrobiol TBD* 20:1–20.

Gruber, S., Groemer, G., and Haider, O. (2019) Inspiring the next generation through the AMADEE-18 MARS analog simulation. *Acta Astronaut* 164:204–211.

Huang, E., Chen, C.H., Huang, T., Lin, E.H., and Xu, J.A. (2000) Raman spectroscopic characteristics of Mg-Fe-Ca pyroxenes. *Am Mineral* 85:473–479.

Klein, C. (2008) *Minerals and Rocks: Exercises in Crystal and Mineral Chemistry, Crystallography, X-ray Powder Diffraction, Mineral and Rock Identification, and Ore Mineralogy*. New York, Wiley. ISBN 13: 9780471772774.

Konstantinidis, M., Cote, K., Lalla, E.A., Zhang, G., Daly, M.G., Gao, X., and Dietrich, P. (2019) On the application of a novel linear mixture model on laser-induced breakdown spectroscopy: implications for Mars. *J Chemom* 33: e3174.

Laetsch, T. and Downs, R. (2006) *Software For Identification and Refinement of Cell Parameters from Powder Diffraction Data of Minerals Using the RRUFF Project and American Mineralogist Crystal Structure Databases*. Kobe, Japan. https://rruff.info/about/about_download.php

Lafuente, B., Downs, R.T., Yang, H., and Stone, N. (2015) The power of databases: the RRUFF project. In: *Highlights in Mineralogical Crystallography*, edited by T. Armbruster and R.M. Danisi, W. De Gruyter, Berlin, Germany, pp 1–30.

Lalla, E., López-Reyes, G., Sansano, A., Sanz-Arranz, A., Schmanke, D., Klingelhöfer, G., Medina-García, J., Martínez-Frías, J., and Rull-Pérez, F. (2015) Spectroscopic analysis and XRD of terrestrial volcanic outcrops on the Tenerife Island as possible Martian analogue. *Estud Geológicos* 71:1–19.

Lalla, E.A., Sanz-Arranz, A., Lopez-Reyes, G., Sansano, A., Medina, J., Schmanke, D., Klingelhoefer, G., Rodríguez-Losada, J.A., Martínez-Frías, J., and Rull, F. (2016) Raman–Mössbauer–XRD studies of selected samples from ''Los Azulejos'' outcrop: a possible analogue for assessing the alteration processes on Mars. *Adv Sp Res* 57:2385–2395.

Lalla, E., Sanz-Arranz, A., Lopez-Reyes, G., Cote, K., Daly, M., Konstantinidis, M., Rodriguez-Losada, J.A., Groemer, G., Medina, J., Martínez-Frías, J., and Rull-Pérez, F. (2019) A micro-Raman and X-ray study of erupted submarine pyroclasts from El Hierro (Spain) and its' astrobiological implications. *Life Sci Sp Res* 21:49–64.

Le Deit, L., Mangold, N., Forni, O., Cousin, A., Lasue, J., Schröder, S., Wiens, R.C., Sumner, D., Fabre, C., Stack, K.M., Anderson, R.B., Blaney, D., Clegg, S., Dromart, G., Fisk, M., Gasnault, O., Grotzinger, J.P., Gupta, S., Lanza, N., Le Mouélic, S., Maurice, S., McLennan, S.M., Meslin, P.-Y., Nachon, M., Newsom, H., Payré, V., Rapin, W., Rice, M., Sautter, V., and Treiman, A.H. (2013) The potassic sedimentary rocks in Gale Crater, Mars, as seen by ChemCam on board Curiosity. *J Geophys Res Planets* 121:784–804.

Lepvrier, C., Fournier, M., Bérard, T., and Roger, J. (2002) Cenozoic extension in coastal Dhofar (southern Oman): implications on the oblique rifting of the Gulf of Aden. *Tectonophysics* 357:279–293.

Léveillé, R. (2009) Validation of astrobiology technologies and instrument operations in terrestrial analogue environments. *Comptes Rendus Palevol* 8:637–648.

Lymer, E.A. (2018) Laser-induced fluorescence spectroscopy as a non-destructive technique for mineral and organic detection in carbonaceous chondrites. MSc thesis, York University, Toronto, Canada. https://yorkspace.library.yorku.ca/xmlui/handle/10315/34546?show=full

Markovski, C., Byrne, J.M., Lalla, E., Lozano-Gorrín, A.D., Klingelhöfer, G., Rull, F., Kappler, A., Hoffmann, T., and Schröder, C. (2017) Abiotic versus biotic iron mineral transformation studied by a miniaturized backscattering Mössbauer spectrometer (MIMOS II), X-ray diffraction and Raman spectroscopy. *Icarus* 296:49–58.

Martin-Islan, J.D. (2004) *Using XPowder: A Software Package for Powder X-Ray Diffraction Analysis*. XpowderX Software Ver 2016.01.15. Platform: Windows. Granada, Spain. ISBN: 978-8416478-87-3.

Marzo, G.A., Davila, A.F., Tornabene, L.L., Dohm, J.M., Fairén, A.G., Gross, C., Kneissl, T., Bishop, J.L., Roush, T.L., and McKay, C.P. (2010) Evidence for Hesperian impact-induced hydrothermalism on Mars. *Icarus* 208:667–683.

Michalski, J.R., Dobrea, E.Z.N.N., Niles, P.B., and Cuadros, J. (2017) Ancient hydrothermal seafloor deposits in Eridania basin on Mars. *Nat Commun* 8:15978.

Morris, R.V, Ruff, S.W., Gellert, R., Ming, D.W., Arvidson, R.E., Clark, B.C., Golden, D.C., Siebach, K., Klingelhöfer, G., Schröder, C., Fleischer, I., Yen, A.S., and Squyres, S.W. (2010) Identification of carbonate-rich outcrops on Mars by the Spirit Rover. *Science* 329:421–424.

National Institute of Standards and Technology (2016) *LIBS Spectral bands NIST—Database*. Available online at http://nist.gov/pml/data/asd.cfm (accessed October 15, 2019).

Palache, C., Berman, H., and Frondel, C. (1952) Dana's System of Mineralogy, 7. ed. *Geol. Föreningen i Stockholm Förhandlingar* 74:218–219.

Popa, C., Carrozzo, F.G., Di Achill, G., Silvestro, S., Esposito, F., and Mennella, V. (2015) First supergene enrichment zone discovered in Shalbatana valley: constrains on martian early atmosphere. EGU General Assembly: Geophysical Research Abstracts Vol. 17, EGU2015–12056, 2015, 4–5. https://ui.adsabs.harvard.edu/abs/2015EGUGA..1712056P/exportcitation; https://meetingorganizer.copernicus.org/EGU2015/EGU2015-12056.pdf

Ramseyer, K., Amthor, J.E., Matter, A., Pettke, T., Wille, M., and Fallick, A.E. (2013) Primary silica precipitate at the Precambrian/Cambrian boundary in the South Oman Salt Basin, Sultanate of Oman. *Mar Pet Geol* 39:187–197.

Reuning, L., Schoenherr, J., Heiman, A., Kukl, P.A., Urai, J.L., and Littke, R. (2007) The salt domes of the Ghaba Salt Basin: An analogue for the hydrocarbon plays of the South Oman Salt Basin. In *13th Bathurst Meeting of Carbonate Sedimentologists Conference*, July 16–18, 2007; Norwich, England. https://doi.org/10.1016/j.orggeochem.2007.03.010.Thrombolites

Robinet, J., Razin, P., Serra-Kiel, J., Gallardo-Garcia, A., Leroy, S., Roger, J., and Grelaud, C., (2013) The Paleogene pre-rift to syn-rift succession in the Dhofar margin (northeastern Gulf of Aden): stratigraphy and depositional environments. *Tectonophysics* 607:1–16.

Roger, J., Platel, J.P., Cavelier, C., and Bourdillon-de-Grissac, C. (1989). New data on the stratigraphy and geological history of Dhofar (Sultanate of Oman). *Bull la Société Géologique Fr V*, 265–277. https://doi.org/10.2113/gssgfbull.V.2.265

Rollinson, H.R., Searle, M.P., Abbasi, I.A., Al-Lazki, A.I., and Al Kindi, M.H. (2014) Tectonic evolution of the Oman Mountains: an introduction. *Geol Soc London Spec Publ* 392:1–7.

Rull-Perez, F. and Martinez-Frias, J. (2003) Identification of calcite grains in the Vaca Muerta mesosiderite by Raman spectroscopy. *J Raman Spectrosc* 34:367–370.

Rull, F., Maurice, S., Hutchinson, I., Moral, A., Perez, C., Diaz, C., Colombo, M., Belenguer, T., Lopez-Reyes, G., Sansano, A., Forni, O., Parot, Y., Striebig, N., Woodward, S., Howe, C., Tarcea, N., Rodriguez, P., Seoane, L., Santiago, A., Rodriguez-Prieto, J.A., Medina, J., Gallego, P., Canchal, R., Santamaría, P., Ramos, G., and Vago, J.L., On Behalf of the RLS Team (2017) The Raman laser spectrometer for the ExoMars Rover Mission to Mars. *Astrobiology* 17:627–654.

Sehlke, A., Mirmalek, Z., Burtt, D., Haberle, C.W., Santiago-Materese, D., Kobs Nawotniak, S.E., Hughes, S.S., Garry, W.B., Bramall, N., Brown, A.J., Heldmann, J.L., and Lim, D.S.S. (2019) Requirements for portable instrument suites during human scientific exploration of Mars. *Astrobiology* 19: 401–425.

Sejkora, N., Sams, S., and Groemer, G. (2018) Geodata workflow for the AMADEE-18 Mars analog mission. *Eur Planet Sci Congr* 12:442.

Storrie-Lombardi, M.C., Muller, J.-P., Fisk, M.R., Cousins, C., Sattler, B., Griffiths, A.D., and Coates, A.J. (2009) Laser-induced fluorescence emission (L.I.F.E.): searching for Mars organics with a UV-enhanced PanCam. *Astrobiology* 9:953–964.

Stromberg, J.M., Parkinson, A., Morison, M., Cloutis, E., Casson, N., Applin, D., Poitras, J., Marti, A.M., Maggiori, C., Cousins, C., Whyte, L., Kruzelecky, R., Das, D., Leveille, R., Berlo, K., Sharma, S.K., Acosta-Maeda, T., Daly, M., and Lalla, E. (2019) Biosignature detection by Mars rover equivalent instruments in samples from the CanMars Mars Sample Return Analogue Deployment. *Planet Space Sci* [Epub ahead of print]; DOI: 10.1016/J.PSS.2019.06.007.

Wang, A., Jolliff, B.L., Haskin, L.A., Kuebler, K.E., and Viskupic, K.M. (2001) Characterization and comparison of structural and compositional features of planetary quadrilateral pyroxenes by Raman spectroscopy. *Am Miner* 86:790–806.

Wang, A., Kuebler, K.E., Jolliff, B.L., and Haskin, L.A. (2004) Raman spectroscopy of Fe-Ti-Cr-oxides, case study: martian meteorite EETA79001. *Am Miner* 89:665–680.

Warren-Rhodes, K.A., Lee, K.C., Archer, S.D.J., Cabrol, N., Ng-Boyle, L., Wettergreen, D., Zacny, K., and Pointing, S.B. (2019) Subsurface microbial habitats in an extreme desert mars-analog environment. *Front Microbiol* 10:69.

Wiens, R.C., Maurice, S., Barraclough, B., Saccoccio, M., Barkley, W.C., Bell, J.F., Bender, S., Bernardin, J., Blaney, D., Blank, J., Bouyé, M., Bridges, N., Bultman, N., Caïs, P., Clanton, R.C., Clark, B., Clegg, S., Cousin, A., Cremers, D., Cros, A., DeFlores, L., Delapp, D., Dingler, R., D'Uston, C., Darby Dyar, M., Elliott, T., Enemark, D., Fabre, C., Flores, M., Forni, O., Gasnault, O., Hale, T., Hays, C., Herkenhoff, K., Kan, E., Kirkland, L., Kouach, D., Landis, D., Langevin, Y., Lanza, N., LaRocca, F., Lasue, J., Latino, J., Limonadi, D., Lindensmith, C., Little, C., Mangold, N., Manhes, G., Mauchien, P., McKay, C., Miller, E., Mooney, J., Morris, R. V, Morrison, L., Nelson, T., Newsom, H., Ollila, A., Ott, M., Pares, L., Perez, R., Poitrasson, F., Provost, C., Reiter, J.W., Roberts, T., Romero, F., Sautter, V., Salazar, S., Simmonds, J.J., Stiglich, R., Storms, S., Striebig, N., Thocaven, J.-J., Trujillo, T., Ulibarri, M., Vaniman, D., Warner, N., Waterbury, R., Whitaker, R., Witt, J., and Wong-Swanson, B. (2012) The ChemCam Instrument Suite on the Mars Science Laboratory (MSL) Rover: body unit and combined system tests. *Space Sci Rev* 170:167–227.

Wiens, R.C., Maurice, S., Mccabe, K., Cais, P., Anderson, R.B., Beyssac, O., Bonal, L., Clegg, S., Deflores, L., Dromart, G., Wiens, R.C., Maurice, S., Mccabe, K., Cais, P., Anderson, R.B., and Supercam Team (2016) The *SuperCam Remote Sensing Instrument Suite for Mars 2020*. In *47th Lunar and Planetary Science Conference*, held March 21–25, 2016 at The Woodlands, TX, LPI Contribution No. 1903, p. 1322. https://ui.adsabs.harvard.edu/abs/2016LPI....47.1322W/abstract

Yuan, Y., Kusky, T.M., and Rajendran, S. (2016) Tertiary and quaternary marine terraces and planation surfaces of northern Oman: interaction of flexural bulge migration associated with the Arabian-Eurasian collision and eustatic sea level changes. *J Earth Sci* 27:955–970.

Address correspondence to:
Emmanuel Alexis Lalla
Centre for Research in Earth and Space Science (CRESS)
York University
4700 Keele Street
Toronto, ON M3J 1P3
Canada

E-mail: elalla@yorku.ca; emmanuel.lalla@oewf.org

Submitted 20 January 2019
Accepted 26 February 2020

Abbreviations Used

BSE = backscattered electron imaging
ChemCam = Chemistry and Camera
CheMin = Chemistry and Mineralogy
DEM = digital model elevation
EDS = energy dispersive spectroscopy
LIBS = laser-induced breakdown spectroscopy
LIF = laser-induced fluorescence
MSL = Mars Science Laboratory
PIL = Planetary Exploration Instrumentation Laboratory
RLS = Raman Laser Spectrometer
SEM = scanning electron microscopy
SHERLOC = Scanning Habitable Environments with Raman and Luminescence for Organics and Chemicals
UV = ultraviolet
XRD = X-ray diffraction